Automated Electrodeposition of Bimetallic Noble-Metal Nanoclusters via Redox-Replacement Reactions for Electrocatalysis

T. S. Mkwizu[a,b], M. K. Mathe[b], and I. Cukrowski[a]

[a]Department of Chemistry, University of Pretoria, NW-1 Building, Pretoria, 0002, South Africa
[b]Energy and Processes Competence Area, Materials Science and Manufacturing Unit, Council for Scientific and Industrial Research (CSIR), PO Box 395, Pretoria, 0001, South Africa

Nanoclusters of bimetallic composition involving platinum with gold or ruthenium were sequentially deposited via redox-replacement of electrodeposited sacrificial Cu adlayers for controlling the deposition of the noble metals. These steps were repeated for a desired number of automated cycles toward: (a) stepwise increase of the size of nanostructures, and (b) stepwise synthesis of the nanostructures in relation to tuning of their electrocatalytic properties. Studies were also performed by eliminating the Cu replacement steps (direct spontaneous deposition) as well as implementing sequential codeposition of the noble-metals with simultaneous Cu redox-replacement steps. Scanning electron microscopy, energy-dispersive X-ray spectroscopy, cyclic voltammetry, chronoamperometry, and electrochemical impedance spectroscopy were implemented to characterize properties of the bimetallic nanoclusters with respect to morphology, elemental composition, and electrocatalytic activity for methanol oxidation. The order of electrocatalytic activity for methanol oxidation in acidic medium was (Ru|Pt) > (Au|Pt) > Pt, in line with the bifunctional mechanism.

Introduction

Nanostructured materials composed of noble-metals have found a great deal of attention for their use as electrocatalysts for instance in energy devices such as fuel cells (1). Development of catalyst fabrication methods is generally carried out in order to reduce the cost of fuel cells; the catalytic activity and utilization efficiency of Pt must be increased and therefore the catalyst layer structure must be modified accordingly and reasonably cheaply. This might be achieved by the catalyst deposition method. In particular, bimetallic catalyst formulations have been a particularly vigorous area of research in direct methanol fuel cells (DMFCs); they have potential applications in portable electronic devices and automobile fuel cells (*1-4*). Pt-based bimetallic catalysts are used to improve the poisoning tolerance of the hydrogen oxidation, or to enhance alcohol oxidation activity in fuel cell anodes (*5-7*) due to their superior activity compared to pure Pt (*1, 8*). The main synthetic challenge for bimetallic electrocatalysts is to have good dispersion and control of the particle sizes as well as maximizing proximity of the primary metallic particles to active areas of electrode surfaces to increase their effective utilization (*1*).

Electrochemical deposition on solid surfaces is a relatively low-cost and efficient method to prepare metal nanoparticles dispersed on solid surfaces. Electrochemical dep

osition has several other advantages compared to other fabrication methods, for instance, the driving force for metal formation from appropriate precursors (the substrate potential) can be controlled more precisely and on a much shorter time scale than in alternative processes (for example, chemical reduction). Electrodeposition of alloys by conventional methods is typically performed with either a preformed layer containing one metal, or codeposition of metals of interest from a common electrolytic bath. The deposition potential or current density, deposition time, and precursor concentrations have to be optimized simultaneously (and often compromised) to deposit the desired bimetallic alloy. Regarding direct deposition of noble-metals, such as Pt, from their dissolved ionic forms, spontaneous (or electroless) deposition may occur at open-circuit conditions, if thermodynamically-favorable potential is established and availability of surface organic (or inorganic) functionalities that may act as electron sinks, a typical scenario on graphitic substrates (9-11). Much better control of nanodeposits might be achieved by sequential deposition of each constituent element from independent precursor solutions to obtain binary systems. Emerging electrodeposition strategies have utilized surface-limited redox-replacement reactions involving spontaneous replacement of less noble, sacrificial elements, such as Cu or Pb, used as templating layers in controlled synthesis of multilayers composed of noble metals.

Formation of monometallic nanoclusters of Pt, Pd and Ag on Au(111) substrate using Cu adlayers as templates have been demonstrated (12). Formation of Pt and Ru monometallic nanofilms on Au(111) substrates has also been shown via repeated redox-replacement cycles. This methodology, also termed Electrochemical Atomic Layer Deposition (EC-ALD), used underpotentially-deposited (UPD) sacrificial Cu or Pb in each cycle to control the formation of monometallic Pt or Ru nanofilms (13, 14). Recently, formation of mixed nanoclusters of Pt-M that were tested for oxygen reduction (M = Au, Pd, Ir, Rh, Re, Ru, or Os) on Pd(111) single-crystal and carbon-supported Pd nanoparticles has been reported (15) whereby UPD Cu was used as template in codeposition of Pt–M by redox-replacement from a common mixture of chloride salts.

The basis of our work was to extend these recent developments in formation of noble-metallic nanostructures via surface-limited reactions. In particular, we have explored automated electrodeposition strategies towards formation of sequentially-deposited bimetallic platinum-based nanoclusters, denoted here as $_n(M|Pt)_{Cu}$/GC to indicate *n* monometallic Pt and M (where M = Au or Ru) adlayers plated over each other by surface-limited redox-replacement (SLRR) reactions of Cu by Pt and M with the nanoclusters supported on a glassy carbon (GC) substrate (This notation also specifies that the first layer deposited on GC was that of Pt, and the last layer deposited (the top layer of a nanocluster) is that of M (where M = Au or Ru). Equivalent codeposited nanoclusters, denoted as $_n(M–Pt)_{Cu}$/GC), were generated from a mixture of Pt and M precursors and allowed simultaneous SLRR of Cu by Pt and M. Monometallic Pt nanoclusters, denoted as $_n(Pt)_{Cu}$/GC, were also generated via SLRR reactions involving Cu and were used as benchmark for electrocatalytic behavior of the bimetallic systems. Moreover, the influence of using Cu SLRR reactions was probed from control experiments that eliminated Cu steps and nanoclusters thus obtained were denoted as $_n(M|Pt)$/GC. Fundamentally, our work posed the following questions: (i) What happens when repeated SLRR reactions are implemented (in a sequential fashion) to grow deposits of two different noble-metals? (ii) How different are deposits obtained by sequential spontaneous deposition (without using any SLRR steps)? (iii) What kind of

deposits are obtained when sequential *codeposition* of noble-metals is implemented using simultaneous SLRR steps? (iv) What electrocatalytic properties do the various deposits impart on reactions that involve bifunctional mechanisms? To this effect, electrocatalysis of methanol oxidation was studied on the various nanostructures and compared to monometallic Pt electrocatalyst synthesized in the same manner as the bimetallic systems.

Experimental

Automated electrodeposition of bimetallic nanoclusters

Automated, sequential and multistage experiments for the formation of mono or bimetallic nanostructures, were achieved with custom–developed LabVIEW (National Instruments, Texas, USA) programs interfaced to 4 piston pumps, an Autolab PGSTAT302 potentiostat/galvanostat, a three-electrode flow-cell, and a 5-way multivalve. The pumps, 5-way valve, and the potentiostat were all computer-controlled via RS–232 and USB standard serial data acquisition interfaces. Four different solutions could be independently delivered to the flow–cell via the outlet channel of the 5–way valve. The flow–cell used had a 120 μL flow–channel (defined by a 1 mm–thick silicone rubber gasket) and it consisted of two Perspex blocks for holding of (i) the reference and working electrode (substrate under study) in the upper block, and (ii) the counter electrode. The Ag/AgCl/3M KCl reference electrode (model 6.0727.000, Metrohm) was placed at the outlet stream of the cell. Unless otherwise stated, all potentials reported here are with respect to this reference electrode. Glassy carbon (GC) substrate was a cylindrical rod (grade V–25, 10 mm diameter, SPI supplies, USA) embedded in a brass holder that was secured via fine threading into the Perspex block, exposing a geometric area of the GC substrate of 0.2 cm^2. The counter electrode was a machined stainless steel rod directly screwed into the Perspex block (exposed geometric area of 0.2 cm^2).

Ultra–high purity nitrogen gas was used to saturate the solutions prior to measurements. N_2 atmosphere was maintained throughout the experiments. Detailed description of the instrumentation has been communicated elsewhere (16).

1 mM Pt^{4+}, Au^{3+}, Ru^{3+} and Cu^{2+} precursor solutions (dissolved in 0.1 M $HClO_4$, which was used as blank electrolyte (BE), at pH 1 ± 0.05) were prepared from H_2PtCl_6, $HAuCl_4$, $RuCl_3$ and $CuSO_4$ salts. All chemicals were of analytical grade (> 99% purity). All solutions were prepared with high–purity water obtained from Milli–Q water purifier system (Millipore Inc. USA) with resistivity of 18 MΩ·cm.

The general electrochemical synthetic strategy (employed to form bimetallic nanoclusters of $_n(M|Pt)_{Cu}$/GC) proceeded as follows: Rinsing the cell with BE), followed by injection of the Cu precursor solution into the cell, followed by Cu deposition at quiescent environment at a pre-set potential (either at underpotential or overpotential). The cell was then rinsed with the BE, filled with the first noble metal precursor (Pt solution) and redox-replacement allowed at open–circuit (OC). The cell was rinsed with BE and Cu deposition proceeded again, followed by rinsing with the second noble-metal solution (Au or Ru solution) and redox-replacement at open circuit, completing one cycle of forming a bimetallic system. These steps were repeated for a desired number of cycles with respect to: (a) stepwise increase of the size of nanostructures, and (b) stepwise synthesis of bimetallic nanostructures in relation to tuning of their catalytic properties. Control experiments were also separately performed by (i) eliminating the Cu steps, or (ii) sequential-codeposition with simultaneous SLRR reactions by two noble metals (Pt

with Ru or Pt with Au). A cartoon of the main scheme to obtain bimetallic nanoclusters, $_n(M|Pt)_{Cu}/GC$, is shown in Figure 1.

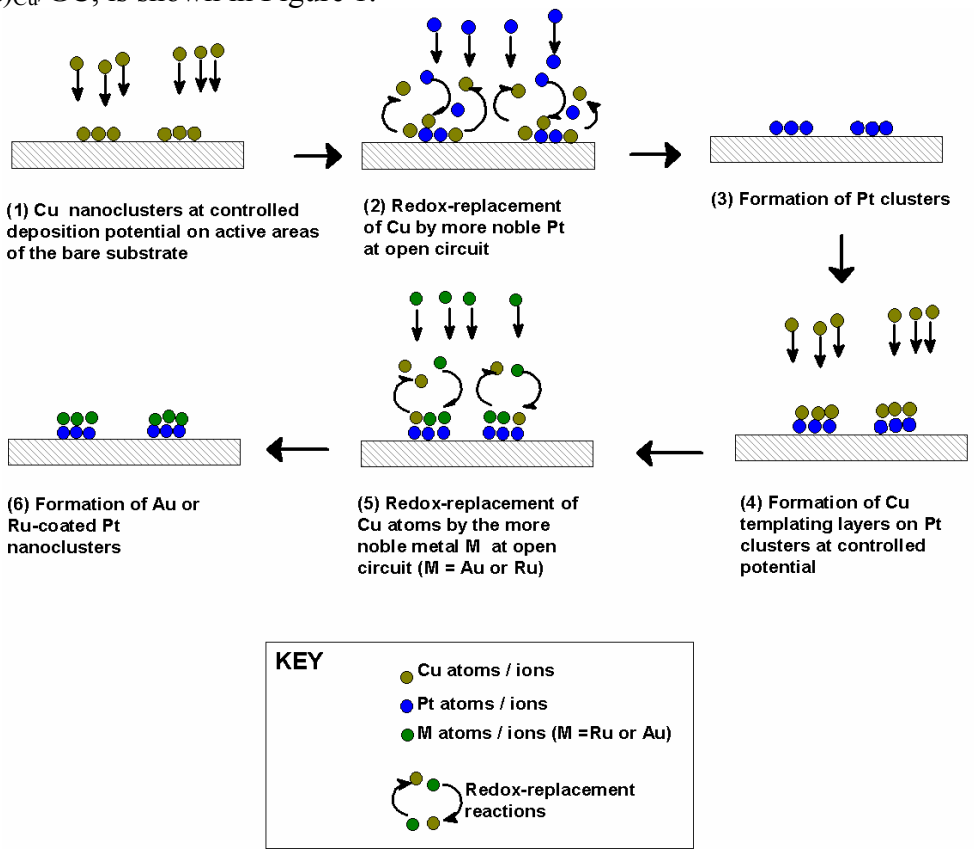

Figure 1. A schematic diagram illustrating electrochemical deposition strategy adopted in this work in formation of bimetallic nanostructured systems M|Pt via surface-limited redox-replacement reactions.

Thermodynamic modelling and characterization of nanostructures

Potential–pH (*E*–pH) models for Pt–Cu–H_2O, Ru–Cu–H_2O , Pt-Au-H_2O, and Pt–Ru–H_2O systems were generated using the thermochemical software package FactSage™ version 5.5 (17).

Electrochemical surface area (ESA) of the modified nanostructured electrodes was estimated in the same flow-cell using: (i) Fe^{2+}/Fe^{3+} couple as an outer sphere redox probe (without exposing the electrode to the ambient) using chronoamperometric experiments ran on N_2-saturated 1 mM $K_4Fe(CN)_6$ (in 0.1 M $HClO_4$) solution under the diffusion-controlled current regime at +0.6 V for 40s. Well-known Cottrell equation (18) was used to estimate ESA values from the chronoamperometric data (corrected for background charge obtained in 0.1 M $HClO_4$ in absence of Fe^{2+} ions; and (ii) linear sweep anodic stripping voltammetry of UPD of copper from potential of +0.05 V held for 90s in 1 mM $CuSO_4$ (in 0.1 M $HClO_4$) solution at scan rate of 50 mV/s. Charges obtained for Cu anodic stripping were corrected for the charge associated with background processes by subtracting the charge deduced for the same electrode under the same deposition and stripping conditions in the background electrolyte (0.1 M $HClO_4$) as described elsewhere (19).

The electrochemical behavior of the nanocluster electrodes were characterized by means of voltammetry in N_2-saturated 0.1 M $HClO_4$ solution. Methanol oxidation studies

were carried out in quiescent N_2-saturated 0.5 M CH_3OH (prepared in 0.1 M $HClO_4$) solutions injected to the electrochemical flow-cell containing the freshly prepared nanocluster electrodes, which were conditioned initially in N_2-saturated 0.1 M $HClO_4$ by scanning the potential at 50 mV/s from –0.2 V to +1.2 V for 5 to 10 cycles. CVs for methanol tests were ran at 50 mV/s for 5 cycles in the potential range from 0 V to +1.0 V, followed by electrochemical impedance spectroscopic measurements in freshly-injected CH_3OH solution, at bias potential of +0.4 V, using sine-wave signal of 10 mV amplitude in the frequency range of 0.5 Hz to 100 kHz. Chronoamperometric measurements were performed at applied potential of +0.4 V for 300s. In between electrochemical measurements the flow-cell was rinsed at open circuit with the blank electrolyte (0.1 M $HClO_4$).

A JEOL model JSM–5800LV scanning electron microscope (operated at 10 kV for SEM imaging and 20 kV for EDX measurements) was employed to study the morphology and to acquire elemental signatures of synthesized nanoclusters *ex situ*.

Results and Discussion

Thermodynamics and electrodeposition involving redox-replacement reactions

Insight onto the effect of pH and potentials on the formation of various Pt, Ru, Au and Cu species, our main goal being deposition of metallic forms, was gained from thermodynamic *E*–pH models for the Pt–Cu–H_2O, Ru–Cu–H_2O, Pt-Ru-H_2O, Au-Cu-H_2O, as well as Pt-Au-H_2O systems at 25 °C for 1 mM solutions. The models showed that (i) metallic Pt exists at *E* smaller than about < +0.9 V at pH between 0 and 3.5, (ii) metallic Pt and Ru co–exist below pH of 1.2 when E < +0.55 V (vs. S.H.E), metallic Cu also exists in the same pH-range but only at potentials below +0.25 V (vs S.H.E), Cu_2O and $Cu(OH)_2$ formed at pH > 4 and *E* > +0.25 (vs S.H.E), (iii) metallic Pt and Au co-existed below pH 7 when *E* < 0.9 V (vs SHE). Based on this information, all deposition experiments were performed at pH of 1 ± 0.05 using 0.1 M $HClO_4$ as background electrolyte where the trend in 'nobility' can be generalized as follows: Au > Pt > Ru > Cu.

Cyclic voltammetry (CV) and anodic stripping voltammetry (ASV) performed on pristine GC in 1 mM $CuSO_4$ (in 0.1 M $HClO_4$), in a wide potential range +0.8 to -0.4 V, showed no Cu deposition in the UPD region. However, Cu UPD is known to take place on Pt, Au and Ru surfaces (20, 21). Therefore, given the Nernst equilibrium potential for the $Cu^{2+} + 2e^- = Cu(s)$, $E_{Cu^{2+}/Cu} = 0.046$ V (versus Ag/AgCl) for 1 mM Cu^{2+} solution, we investigated the use of SLRR steps involving Cu (for subsequent replacement by the more noble Pt, Au, or Ru) electrodeposited either at a slight overpotential (-0.05 V versus Ag/AgCl) or underpotential (+0.05 V versus Ag/AgCl),). Effect of Cu deposition time (t_{dep}) on GC-substrate was probed by running ASV, employing deposition potential –0.05 V, for t_{dep} ranging from 5 to 150 s. Calculations of monolayer-equivalent amounts retrieved from integration Cu oxidation currents led to deduction that about 1 monolayer-equivalent of Cu nanoclusters was obtained after t_{dep} of about 90 s. Studies performed elsewhere on Cu electrodeposition on GC substrate (22) indicate that fast electrocrystallisation of well–dispersed Cu nanoclusters occurs at kinetically–controlled deposition overpotentials of Cu. Moreover, using Cu SLRR steps with the Cu adlayers generated at overpotentials has been noted elsewhere in generated monometallic Pt nanostructures on a bulk Au electrode via a Cu SLRR step (23). The main unique

extension implemented in our work was to apply SLRR steps for deposition of two different noble metals deposited sequentially and individually via a Cu SLRR step that was repeated to increase the size of nanoclusters, with the final aim of multiplying bimetallic active sites for effective synergistic effects for electrocatalytic applications.

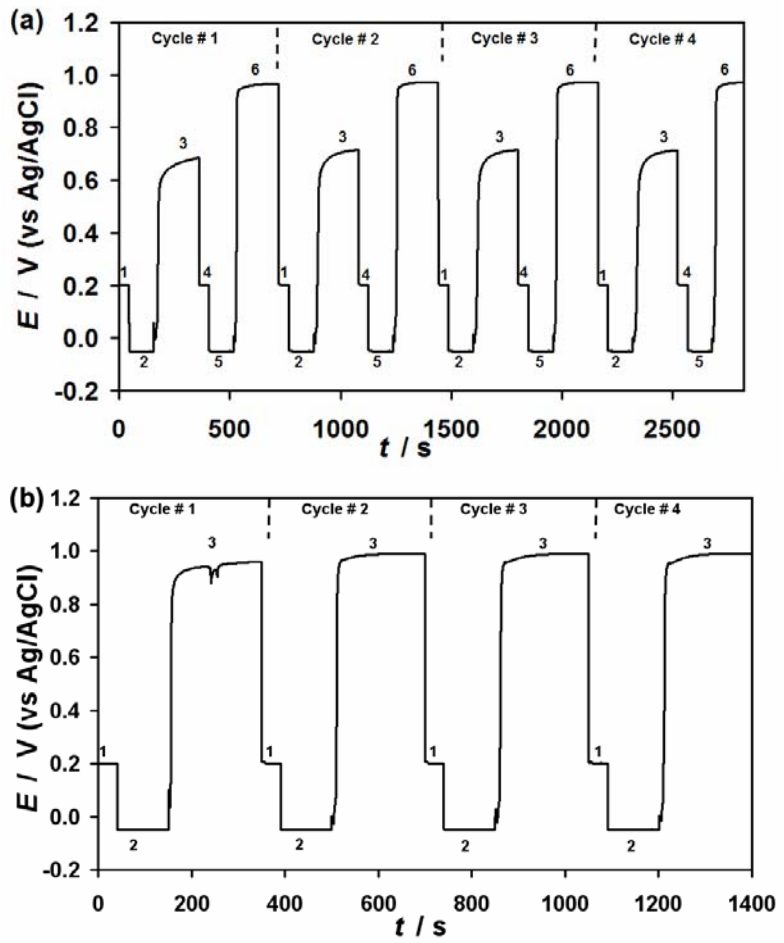

Figure 2. Potential-time (*E–t*) graphs recorded during several cycles of SLRR steps involving Cu with Pt and Au to obtain (a) $_n(Au|Pt)_{Cu}$/GC whereby SLRR steps involving Cu OPD at -0.05 V were implemented, and (b) sequentially-codeposited $_n(Au–Pt)_{Cu}$/GC nanoclusters with simultaneous SLRR steps involving Cu OPD at -0.05 V. See text for details.

Having considered the nature of Cu deposition on the GC substrate (with the aim of the surface-limited redox–replacement by more noble Pt, Au or Ru) and assuming the preferential redox-reaction pathways leading to zero-valent metallic states, and fast kinetics of the redox processes, with the main limiting factor being availability of electrons from Cu redox-replacement by the noble metals, SLRR steps were implemented as described by Equations 1-4:

$$GC + Cu^{2+} + 2e^- \longrightarrow Cu/GC \quad [1]$$

$$2Cu/GC + PtCl_6^{2-} \longrightarrow Pt/GC + 2Cu^{2+} + 6Cl^- \quad [2]$$

$$Pt/GC + Cu^{2+} + 2e^- \longrightarrow Cu(Pt)/GC \quad [3]$$

$$3Cu(Pt)/GC + 2Ru^{3+} \rightarrow 2Ru(Pt)/GC + 3Cu^{2+} \quad [4a]$$

or

$$3Cu(Pt)/GC + 2AuCl_4^- \rightarrow 2Au(Pt)/GC + 3Cu^{2+} + 8Cl^- \quad [4b]$$

The following electrochemical parameters were selected for each stage employed to generate the ${}_n(M|Pt)_{Cu}/GC$ electrode – see Figure 2a: (1) rinsing the flow cell with BE at E = +0.2 V (applied potential to the GC working electrode for cleaning and conditioning purposes) for 20 s, followed by rinsing with the Cu(II) solution at the same potential, a potential at which Cu(s) could not deposit, for 20 s; (2) Cu deposition at E_{dep} = –0.05 V (OPD) or +0.05 V (UPD) for 90 s, followed by rinsing with BE at E_{dep} for 20 s; (3) rinsing with the Pt^{4+} precursor solution at OC for 20 s, followed by the OC redox-replacement by Pt at quiescent conditions for 180 s; (4) rinsing, initially with BE, followed by the Cu solution, at E = +0.2 V for 20 s for both solutions; (5) Cu deposition at E_{dep} = –0.05 V for 90 s, followed by rinsing with BE at the same potential for 20 s; (6) rinsing with either Ru^{3+} (or $AuCl_4^-$) precursor solutions at OC for 20 s, followed by the OC SLRR reaction by Ru (or Au) at quiescent conditions for 180 s. This protocol was repeated for up to 8 cycles to generate larger bimetallic nanoclusters. It should be understood that, in the case of the use of Cu UPD (which does not happen on pristine GC for the experimental conditions employed in this work), spontaneously formed Pt during the first cycle on fresh GC determined the subsequent Cu UPD cycles.

Cycles in the control experiments were as follows: (i) the sequentially-deposited ${}_n(Pt)_{Cu}/GC$ and sequentially-codeposited ${}_n(M–Pt)_{Cu}/GC$ nanoclusters – they were generated by cycles which maintained stages 1 and 2 exactly the same as employed for the generation of the ${}_n(M|Pt)_{Cu}/GC$ nanoclusters; stage 3 was performed with a precursor solution containing $PtCl_6^{2-}$ to form monometallic Pt or a mixed solution of $PtCl_6^{2-}$ with either Ru^{3+} (towards codeposition of Ru–Pt nanoparticles) or $AuCl_4^-$ (to form Au–Pt) – see Figure 2b; (ii) the ${}_n(M|Pt)/GC$ nanocluster electrode, without the use of sacrificial copper, was obtained by performing the same sequence of stages as for ${}_n(M|Pt)_{Cu}/GC$ described above with exclusion the Cu solution at stages 1’ and 4’ which were replaced by the BE solution, and background deposition at stages 2’ and 5’ – see currrent–potential–time (*i*-*E*-*t*) transients recorded during various deposition cycles in Figure 3.

Figure 4 presents variations in maximum open–circuit potential (OCP) during Pt, and M (M = Au or Ru) redox-exchange reactions with Cu (stages 3 and 6 in Figures 2 and 3) to form ${}_n(M|Pt)_{Cu}/GC$. It is clearly seen that there are distinctive processes taking place that might be used as signatures for the Cu redox-replacement reactions by Pt or metal M. The OCP during Pt redox-exchange reaction reached a maximum and constant value of about +0.65 V. The OCP during Au redox-exchange was steady at a value of about +0.95 V, regardless of the nature of Cu deposition (either at UPD or OPD). It is clear that metallic Pt(s) and Au(s) are indeed deposited on the GC substrate when *E*-*t* transient of stage 3 in Figure 4 is compared with equilibrium potentials for the $Pt^{2+}/Pt(s)$ and $Au^{3+}/Au(s)$ redox-couples; metallic Pt(s) and Au(s); for most of the deposition time, the OCP is within the potential range where Pt(s), Au(s) and Cu^{2+} are thermodynamically predicted to co-exist and a possibility of co-existence of Pt(s), Pt^{2+} and Cu^{2+} might only be considered when the OCP reaches its maximum value in stage 3.

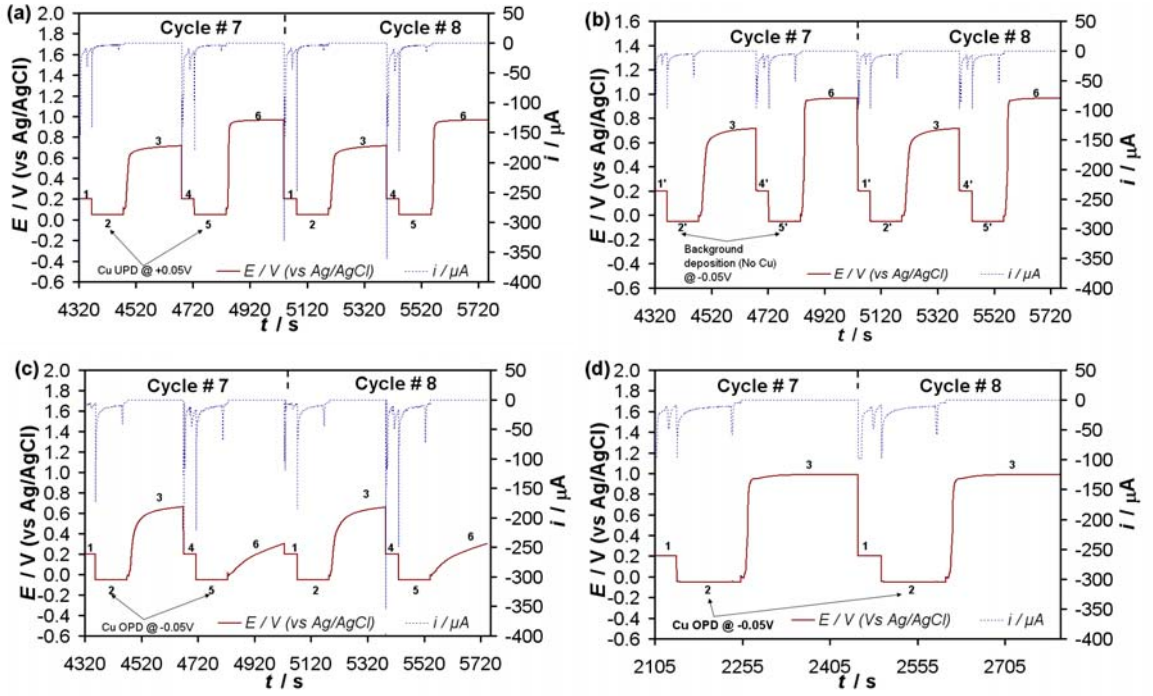

Figure 3. Current-potential-time (*i–E–t*) transients recorded during deposition cycles to obtain: (a) $_n(Au|Pt)_{Cu}$/GC nanoclusters using SLRR steps involving Cu UPD at +0.05 V; (b) $_n(Au|Pt)$/GC nanoclusters using sequential spontaneous deposition with background deposition (in the absence of Cu^{2+}) at –0.05 V at stages 2' and 5'; (c) $_n(Ru|Pt)_{Cu}$/GC nanoclusters using SLRR steps involving Cu OPD at –0.05 V; (d) sequentially-codeposited $_n(Au–Pt)_{Cu}$/GC with SLRR steps involving Cu OPD at –0.05 V.

In case of Ru deposition, the OC potential approaches a value of about +0.45 V in the first cycle and gradually decreases reaching a constant maximum value of about +0.32 V (see Figure 4c). The variation in the maximum value of the OCP during the Ru deposition suggests that initially, besides Ru(s), RuO_2 might also be formed, but after the fifth cycle the only thermodynamically predicted equilibrium involves Ru(s) and Cu^{2+}. From this discussion one might conclude that deposition of monometallic clusters of Pt(s), Au(s) and Ru(s) takes place only when Cu SLRR steps were carried out. OCP reached during simultaneous SLRR by two noble-metals (see Figure 4e) significantly favor the deposition of the more noble-metal. For instance, the OCP during codeposition of Ru and Pt reached a value of about +0.48 V, well within the potential windows where Pt(s) and RuO_2(s) are thermodynamically predicted to coexist with Cu^{2+}. During Au and Pt codeposition maximum OCP reached a steady value of about + 0.95 V, significantly in favor of Au^{3+}/Au(s) equilibrium potential.

Figure 5 presents variation in total charge (uncorrected for background current) determined from integration of current-time (*i–t*) curves at stages 2 and 4 during Cu deposition at various cycles in deposition of $_n(M|Pt)_{Cu}$/GC nanoclusters. There is a clear difference for the first cycle, during which Cu deposits on pristine GC substrate as compared to subsequent cycles for which Cu deposits on formed Pt, Au or Ru nuclei. We observe a gradual increase of the Cu charge with increasing number of cycles, with a tendency to a steady value after the first 3 cycles, probably indicating more uniform Cu deposition on the well-developed noble metal clusters. As expected, larger values of charge also developed when OPD Cu was used as compared to UPD Cu, several different

adlayers of Cu were deposited at OPD whereas monolayers or less were deposited at UPD.

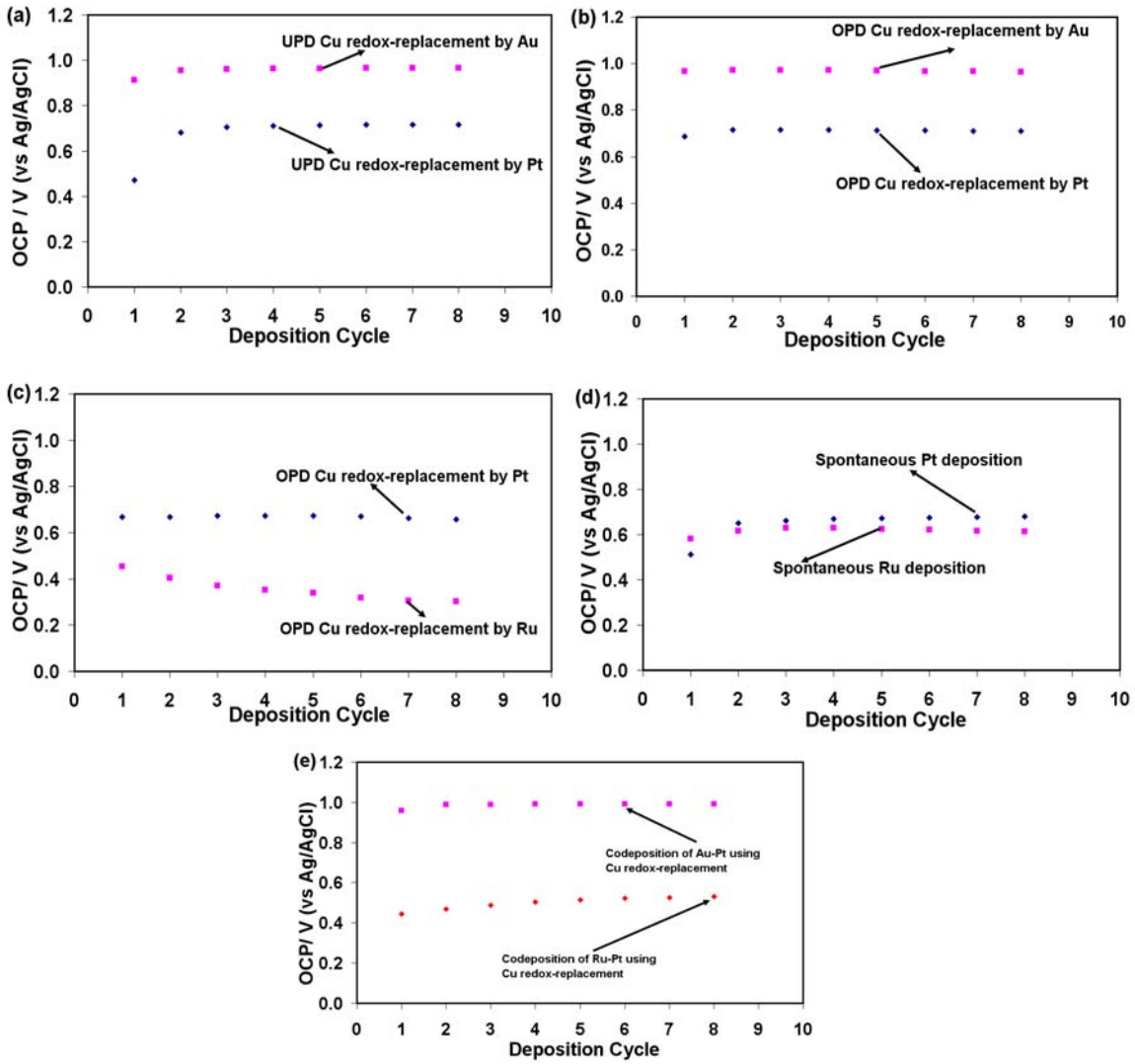

Figure 4. Variation in maximum open-circuit potential (OCP) attained during Pt and M (M = Au or Ru) sequential deposition to generate: (a) – (b) $_n(Au|Pt)_{Cu}$/GC nanoclusters; (c) $_n(Ru|Pt)_{Cu}$/GC nanoclusters; (d) $_n(Ru|Pt)_{Cu}$/GC nanoclusters; and (e) sequentially–codeposited $_n(Ru–Pt)_{Cu}$/GC and $_n(Au–Pt)_{Cu}$/GC nanoclusters.

Electrochemical characterization

Typical CVs the as-prepared nanoclusters are shown in Figure 6. They confirmed that (i) Pt, Au or Ru electrochemically-active sites were generated (well-known electrochemical signature of Pt and Au electrodes (18, 24) in acidic medium were observed), (ii) CVs performed with electrodes generated in the presence and absence of Ru or Au confirm incorporation of gold and ruthenium by comparing the recorded voltammograms in the potential window +0.8 to +1.2 V; in the case of $_n(Ru|Pt)_{Cu}$/GC electrode a rapid rise in oxidation current is observed in the mentioned potential range that is consistent with electrochemical formation of surface RuO_2 which is considered a reversible oxide at potentials below +1.3 V (vs Ag/AgCl) as noted elsewhere (25),

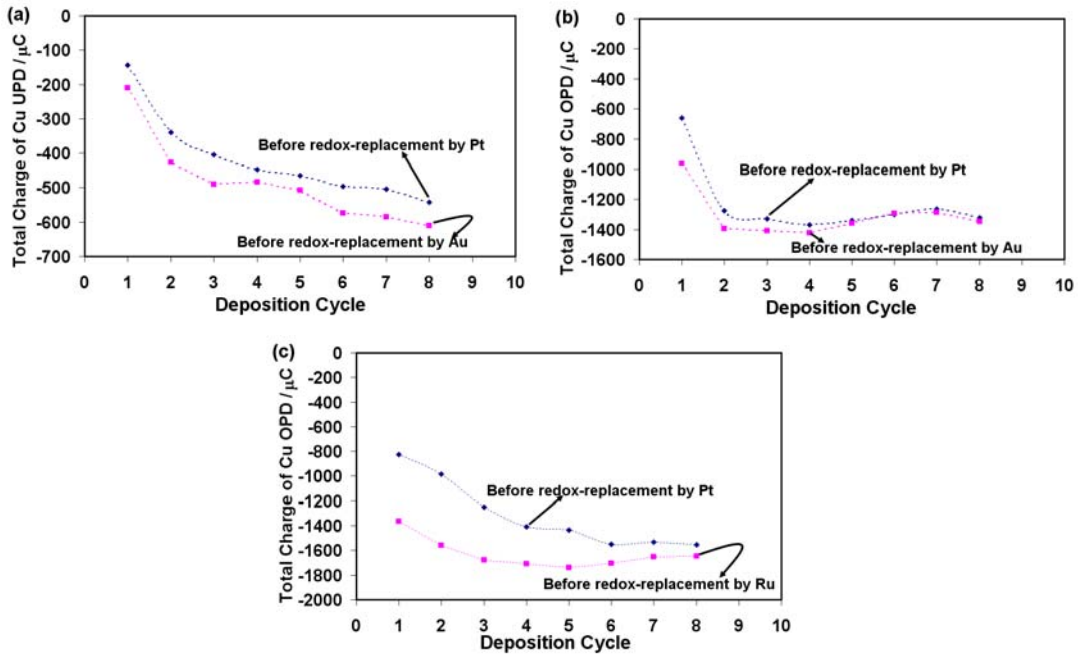

Figure 5. Variation in total charge developed during Cu deposition stages at various deposition cycles prior redox-exchange by Pt and M (M = Au or Ru) surface-limited redox-replacement (SLRR) reaction stages during sequential deposition to generate (a) $_n(Au|Pt)_{Cu}$/GC nanoclusters using SLRR steps involving UPD Cu deposited at +0.05 V; (b) $_n(Au|Pt)_{Cu}$/GC nanoclusters using SLRR steps involving OPD Cu deposited at –0.05 V; (c) $_n(Ru|Pt)_{Cu}$/GC nanoclusters using SLRR steps as in (b).

(iii) more surface-active Pt and Au sites were generated in the case of individually deposited Pt and Au via SLRR steps (to generate the $_n(Au|Pt)_{Cu}$/GC system) as compared to sequential-codeposition of the noble-metals (to produce $_n(Au–Pt)_{Cu}$/GC). This can be appreciated by inspection of the pronounced Au and Pt oxides reduction peaks at + 1.0V and +0.5 V respectively, on the $_n(Au|Pt)_{Cu}$/GC system in Figure 6a, and (iv) comparison of monometallic $_n(Pt)_{Cu}$/GC and bimetallic $_n(Ru|Pt)_{Cu}$/GC electrodes (see Figure 6b) reveal that electrochemical and catalytic properties of Pt(s) have not been influenced by deposited Ru adlayers, in the case of $_n(Ru|Pt)_{Cu}$/GC, as indicated by almost identical hydrogen adsorption/desorption peaks in the potential range 0 V to –0.2 V (see Figure 6b).

To further probe the active surfaces of the generated nanocluster electrodes, we utilized the coulometric methodologies involving UPD Cu anodic stripping voltammetry and chronoamperometry involving Fe^{2+}/Fe^{3+} redox couple as probes to estimate active surface area (ASA) and overall electrochemical surface area (ESA), respectively. Figure 7 displays typical cyclic voltammograms of bare glassy carbon (GC) electrode and the various Pt, Au|Pt, and Ru|Pt nanostructured electrodes (obtained using OPD Cu SLRR steps) recorded in 0.1 M $HClO_4$ solution in the presence and absence of 1 mM $CuSO_4$. As stated earlier, no Cu UPD features are observed on bare GC only bulk copper deposition and stripping are observed (Figure 7a) as commented earlier. In all the other cases (Figures 7b to 7d) involving monometallic Pt or bimetallic electrodes (Au|Pt and Ru|Pt), both deposition as well as stripping of underpotential-deposited and bulk Cu are observed on the modified electrodes in the potential ranges about +0.5 V to –0.2 V, whereby in the

cathodic scan, Cu UPD features are identifiable in the potential range about +0.5 V to +0.05 V, albeit slightly distorted by platinum and ruthenium oxides reduction waves (seen in the dashed curves that were recorded in the absence of Cu^{2+} ions – see Figure 7). This is in agreement with the known electrochemistry of Cu UPD on Pt, Au and Ru electrodes (21, 26).

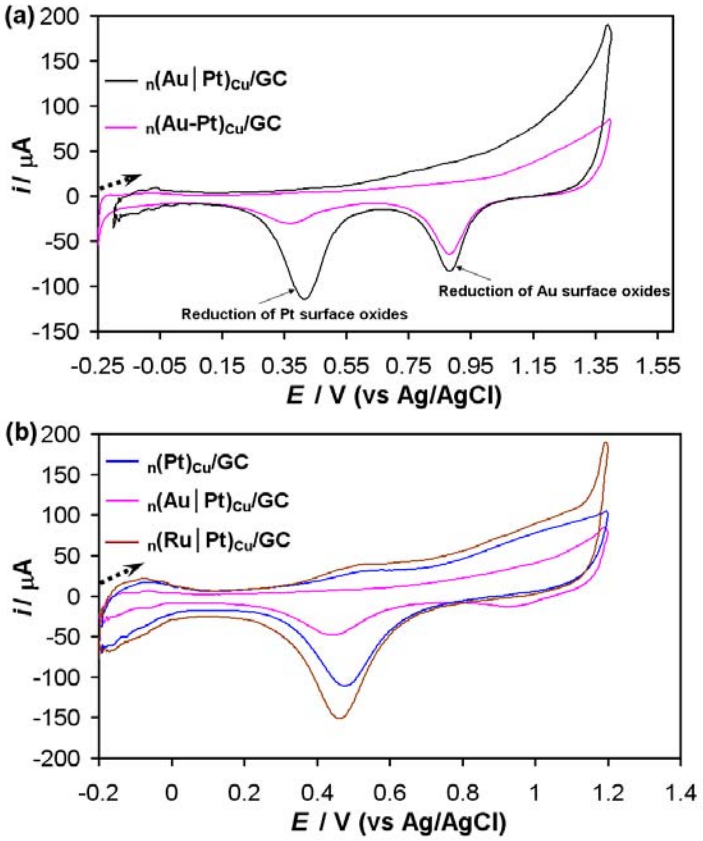

Figure 6. Cyclic voltammetric (CV) responses of the various as-prepared nanoclusters recorded in N_2-saturated 0.1 M $HClO_4$ electrolyte. (a) CV responses of $_n(Au|Pt)_{Cu}$/GC and the codeposited $_n(Au–Pt)_{Cu}$/GC nanoclusters obtained after 8 deposition cycles. (b) Comparison of CV responses of $_n(Pt)_{Cu}$/GC, $_n(Au|Pt)_{Cu}$/GC, and $_n(Ru|Pt)_{Cu}$/GC nanoclusters obtained after 8 deposition cycles via SLRR steps involving Cu OPD at –0.05 V. Scan rate was 50 mV/s in all cases and 5th cycles were taken for this analysis.

Typical linear sweep anodic stripping voltammograms of UPD Cu, deposited at +0.05 V for 90s using 1 mM Cu^{2+} in 0.1 M $HClO_4$ on the Pt and M|Pt systems are shown in Figure 8. Calculations of the active surface area were carried out by integrating the potential-current curves, corrected for the background current, to obtain UPD Cu stripping charge, and using a conversion factor of 420 μC cm^{-2} (21, 26), as the charge due to copper UPD layer on polycrystalline platinum-ruthenium surfaces. Table I summarizes the estimated surface areas.

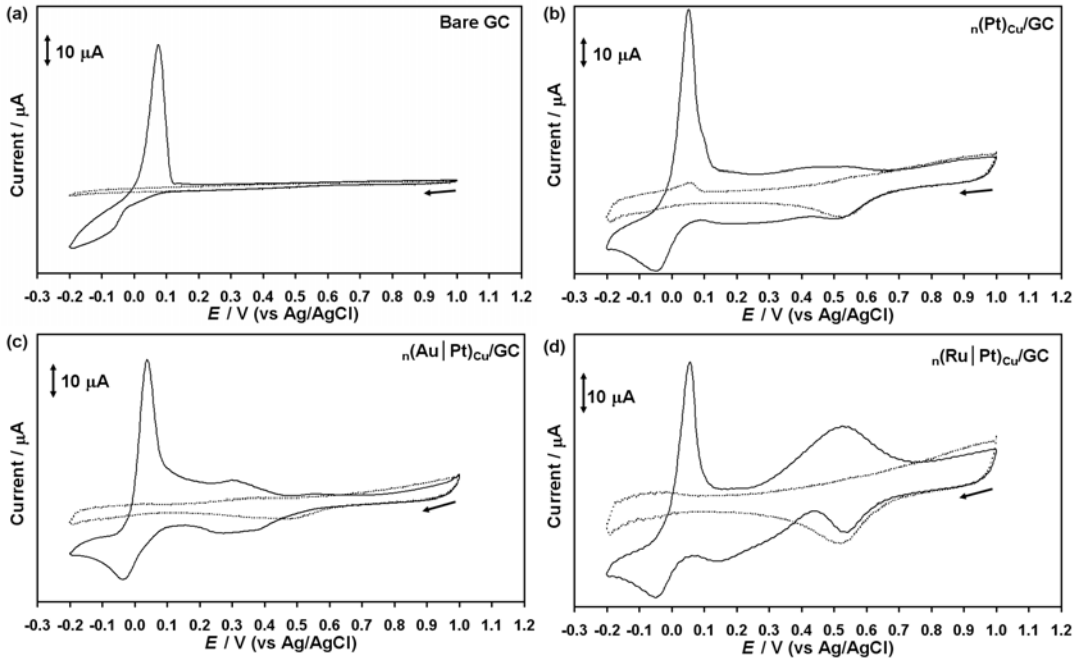

Figure 7. Cyclic voltammetric (CV) responses recorded in N_2-saturated 0.1 M $HClO_4$ electrolyte (dashed lines) and 1 mM $CuSO_4$ and 0.1 M $HClO_4$ solution (solid lines) on (a) bare GC, (b) $_n(Pt)_{Cu}$/GC, (c) $_n(Au|Pt)_{Cu}$/GC, (d) $_n(Ru|Pt)_{Cu}$/GC nanoclusters obtained after 8 deposition cycles via SLRR steps involving Cu OPD at –0.05 V. Scan rate was 5 mV/s in all cases. Arrows indicate starting potential and initial scan direction.

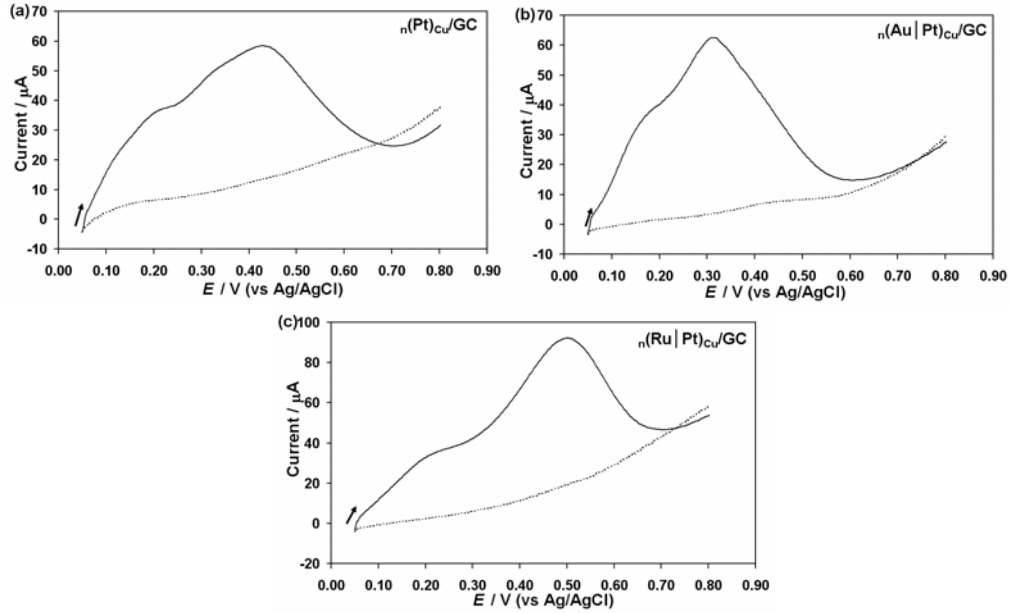

Figure 8. Anodic stripping voltammetry for Cu UPD deposited at +0.05 V for 90s on various nanoclusters obtained as described in Figure 7 to deduce active surface area for (a) $_n(Pt)_{Cu}$/GC, (b) $_n(Au|Pt)_{Cu}$/GC, and (c) $_n(Ru|Pt)_{Cu}$/GC nanoclusters. In all cases, scan rate was 50 mV/s.

Table I. Copper stripping charge and active surface area (ASA) values obtained using UPD Cu method and electrochemical surface area (ESA) values using Fe^{2+}/Fe^{3+} redox probe

	Cu UPD method		Fe^{2+}/Fe^{3+} probe
Electrode	**Stripping Charge (μC)**	**ASA (cm^2)**	**ESA (cm^2)**
$_n(Pt)_{Cu}/GC$	322	0.766	0.244
$_n(Au\|Pt)_{Cu}/GC$	344	0.819	0.250
$_n(Ru\|Pt)_{Cu}/GC$	487	1.160	0.256

* Electrodes generated using deposition cycles as in Figure 7.

Since the geometric area of the bare GC electrode was 0.2 cm^2, the estimated ESA using the outer-sphere Fe^{2+}/Fe^{3+} redox probe indicate a slight increase in the surface area due to deposited metals in addition to the bare areas of the GC surface which are also responsive to the Fe^{2+}/Fe^{3+} redox action. However, using the Cu UPD method, which in principle does not involve deposition on bare GC sites (see Figure 7a) at the UPD applied potential of +0.05 V, the estimated ASA values obtained were about four- to six-fold larger than the geometric area of the bare GC (see Table I), suggesting high-surface-area nanoclusters with high aspect ratios were generated. The most surface-active electrode was bimetallic Ru|Pt followed by Au|Pt and the least active was monometallic Pt.

Microscopic characterization

Figure 9 presents representative SEM images and corresponding EDX spectra for the $_n(Au|Pt)_{Cu}/GC$ decorated electrodes obtained either with Cu UPD SLRR reactions (Figure 9(a)), or Cu OPD SLRR reactions (Figure 9(b)). Figure 9(c) shows the sequentially-codeposited Au-Pt nanoclusters. Elemental signatures for Pt and Au were clearly observed. It is seen from Figure 9 that reasonably uniform coverage of the GC substrate by deposited nanoparticles was obtained after 8 deposition cycles with the GC surface providing electrochemically active sites for a preferential growth of the nanoclusters. Finely dispersed nanoclusters were formed in the case of Au|Pt sequentially generated using separate Cu SLRR steps for either Pt or Au (Figure 9a and 9b). The use of either Cu UPD or Cu OPD as templating adlayers led to much finer nanoclusters, especially in the case of Cu UPD. This is in line with the fact that multilayers of Cu were generated at OPD and their replacement led to multilayers of Pt and Au upon SLRR steps by these more noble metals, as opposed to smaller number of adlayers (presumably monolayers or submonolayers) that had to be replaced when Cu UPD SLRR steps were used. Significant agglomerated particles were formed in the case of the sequentially-codeposited Pt-Au (Figure 9c).

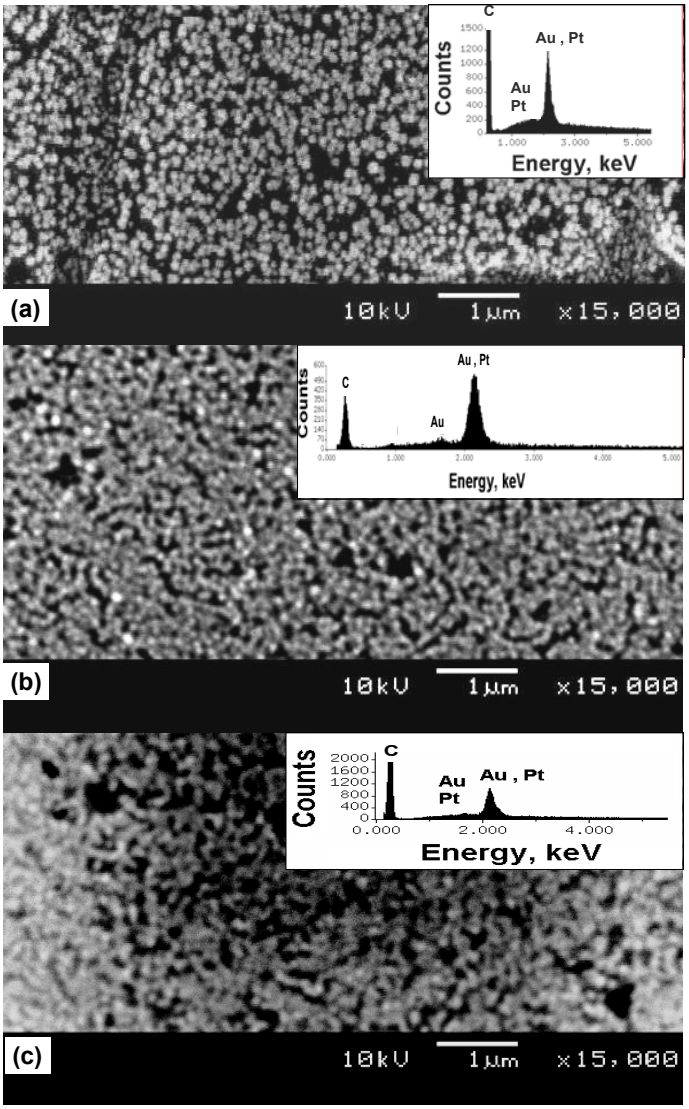

Figure 9. SEM micrographs and corresponding EDX spectra (insets) of: (a) bimetallic $_n(Au|Pt)_{Cu}$/GC nanoclusters obtained after 8 sequential deposition cycles with SLRR reactions involving *Cu UPD*; (b) bimetallic $_n(Au|Pt)_{Cu}$/GC nanoparticles obtained after 8 sequential deposition cycles with SLRR reactions involving *Cu OPD*; (c) sequentially-codeposited Au–Pt nanostructures obtained with simultaneous Cu OPD SLRR reactions after 8 deposition cycles.

Electrocatalytic oxidation of methanol

Comparative studies on monometallic Pt and bimetallic (Ru|Pt) and (Au|Pt) Pt (to evaluate their electrocatalytic activity to oxidize methanol) were performed for the nanoclusters obtained using Cu SLRR steps. Generally accepted reaction mechanism for methanol oxidation in acidic media on bimetallic platinum-based catalysts may be described by Equations 5 to 8 (1, 27, 28). Methanol molecules are preferentially adsorbed only on Pt(s) active sites, followed by subsequent de–hydrogenation reaction (Equations. 5–6). The interaction between CH_3OH and the non-platinum metal M(s) is a strongly activated process correlated with a high energy of adsorption of oxygen on M(s). However, water dissociates more easily on Ru(s) or Au(s) than on Pt(s) resulting in OH_{ads}

(Equation 7). The species, CO_{ads} and OH_{ads}, adsorbed on adjacent Pt(s) and M(s) particles combine together forming CO_2 (Equation 10) in a Langmuir–Hinshelwood (L–H) type reaction (1).

$$Pt + CH_3OH \rightarrow Pt - (CH_3OH)_{ads} \quad [5]$$

$$Pt - (CH_3OH)_{ads} \rightarrow Pt - (CO)_{ads} + 4H^+ + 4e^- \quad [6]$$

$$H_2O + M \rightarrow M - OH_{ads} + H^+ + e^- \quad [7a]$$

$$H_2O + Pt \rightarrow Pt - OH_{ads} + H^+ + e^- \quad [7b]$$

$$Pt - CO_{ads} + M - OH_{ads} \rightarrow Pt + M + CO_2 + H^+ + e^- \quad [8a]$$

$$Pt - CO_{ads} + Pt - OH_{ads} \rightarrow 2Pt + CO_2 + H^+ + e^- \quad [8b]$$

(M = Ru or Au)

Typical CVs recorded on the N_2-saturated 0.5 M CH_3OH (in 0.1 M $HClO_4$) solution at scan rate of 50 mV/s for three electrocatalysts generated by use of the sacrificial copper layers, the $_n(Pt)_{Cu}$/GC, $_n(Ru|Pt)_{Cu}$/GC, and $_n(Au|Pt)_{Cu}$/GC, obtained after 8 deposition cycles are shown in Figure 10. In this case the current density (*j*) = current (*i)* / Active Surface Area (ASA). ASA determined using the method involving UPD of Cu (Table I). The onset potentials on the CVs for the monometallic and bimetallic systems synthesized with the same deposition parameters clearly showed a shift from about +0.45 V for the $_n(Pt)_{Cu}$/GC electrode, to about +0.40 V for the $_n(Ru|Pt)_{Cu}$/GC electrode. Also, a significant increase in current density is observed for the bimetallic system Ru|Pt. However, the forward and reverse peak potentials appear to be very much the same for all electrocatalysts suggesting that the overall reaction mechanism of methanol oxidation is the same with largely increased catalytic activity in case of Ru|Pt and Au|Pt nanoclusters. The same trend was observed even when current density values were generated using either the ESA from Fe^{2+}/Fe^{3+} probe or geometric area of the GC, suggesting that the bifunctional electrocatalytic processes play significant role in the electrocatalysis of CH_3OH by the investigated bimetallic nanocluster electrodes. These observations agree with those made elsewhere in the literature on the promotional effects induced on Pt(s) by Ru(s) or Au(s) leading to decrease in the overpotential for methanol oxidation in line with the bifunctional mechanism (29, 30). Similar trends in electrocatalytic activity were also observed using additional electrochemical techniques (results not shown). For instance, using chronoamperometry, current densities observed at applied potential of +0.4 V for 300s in 0.5 M CH_3OH (in 0.1 M $HClO_4$) increased in the order the order Pt< Au|Pt < Ru|Pt. Moreover, charge-transfer resistance (R_{ct}) obtained from electrochemical impedance spectroscopy (performed at + 0.4 V in the CH_3OH solutions) correspond well with the above order of electrochemical activity, that is, the Ru|Pt system had the lowest R_{ct} compared to Au|Pt, the highest value being that for monometallic Pt.

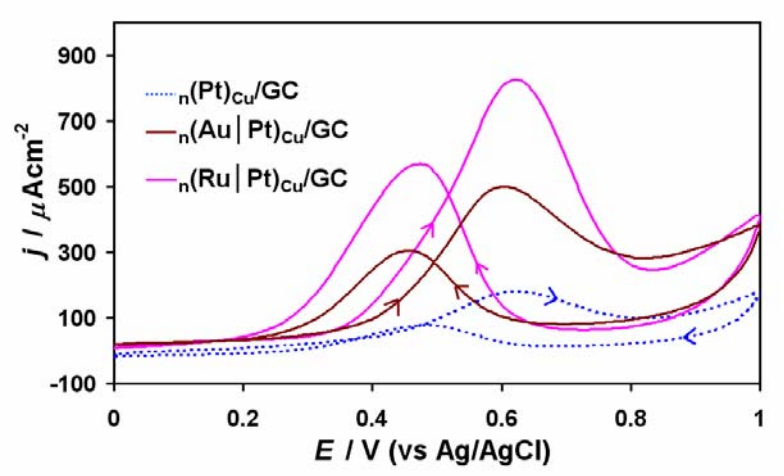

Figure 10. Cyclic voltammograms of nanoclusters (prepared as described in Figure 7) in Nitrogen-saturated 0.5 M CH_3OH and 0.1 M $HClO_4$. Scan rate = 50 mV/s. The start potential was 0 V and scans were carried out in the anodic direction to +1 V (as indicated by the arrows), followed by cathodic direction from +1 V back to 0 V. 5^{th} cycles were taken for this analysis.

Conclusions

It has been demonstrated that it is possible to synthesize highly-surface active bimetallic platinum-ruthenium and platinum-gold nanoclusters via a three–step, automated sequential electrodeposition methodology utilizing surface–limited redox replacement reactions of Cu by the more noble metals Pt , Au and Ru. The presence of sacrificial copper, has been proved to be a necessary condition for the deposition of metallic layers of ruthenium on metallic platinum; the control experiments, where copper was not used, proved that most likely RuO_2(s) instead of Ru(s) is spontaneously plated on metallic Pt. Moreover, codeposition with SLRR steps generally disfavored formation of metallic forms of the lesser noble-metal such as Ru or Pt with respect to the nobler Au. Moreover, the use of stepwise SLRR steps in deposition of bimetallic systems leads to finer nanoclusters, which are more surface-active compared to nanoparticles obtained via codeposition with simultaneous SLRR steps. Electrocatalytic studies on the various decorated GC electrodes showed that bimetallic nanostructures obtained M|Pt (M = Au or Ru) were more active than monometallic Pt toward CH_3OH oxidation and the general order of activity to oxidize methanol was: Pt< Au|Pt < Ru|Pt.

Acknowledgments

Research facilities availed by University of Pretoria and financial support provided by CSIR under a parliamentary grant (Project No. HTR018P), are gratefully acknowledged.

References

1. M. Watanabe, in *Catalysis and Electrocatalysis at Nanoparticle Surfaces*, A. Wieckowski, E. R. Savinova, C. G. Vayenas, Editors,. p. 827, CRC Press, Boca Raton (2003).

2. J. Mathiyarasu, A. M. Remona, A. Mani, K. L. N. Phani, V. Yegnaraman, *J. Solid State Electrochem.*, **8**, 968 (2004).
3. M. T. M. Koper, *Surf. Sci.*, **548**, 1 (2004).
4. P. Costamagna, S. Srinivasan, *J. Power Sources*, **102**, 242-252 (2001).
5. F. Vigier, S. Rousseau, C. Coutanceau, J. Leger, C. Lamy, *Top. Catal.*, **40**, 111 (2006).
6. W. Goddard *et al.*, *Mol. Simul.*, **32**, 251 (2006).
7. E. Antolini, *J. Power Sources*, **170**, 1 (2007).
8. T. Toda, H. Igarashi, M. Watanabe, *J. Electroanal. Chem.*, **460**, 258 (1999).
9. J. V. Zoval, J. Lee, S. Gorer, R. M. Penner, *J. Phys. Chem. B*, **102**, 1166 (1998).
10. F. A. Uribe, F. H. Garzon, E. L. Brosha, C. M. Johnston, S. D. Conradson, and M. S. Wilson, *J. Electrochem. Soc.* **154**, D623 (2007).
11. P. Shen, N. Chi, K. Chan, D. L. Phillips, *Appl. Surf. Sci.*, **172**, 159 (2001).
12. S. R. Brankovic, J. X. Wang, R. R. Adzic, *Surf. Sci.*, **474**, L173 (2001).
13. Y.-G. Kim, J. Y. Kim, D. Vairavapandian, J. L. Stickney, *J. Phys. Chem. B*, **110**, 17998 (2006).
14. C. Thambidurai, Y. Kim, J. L. Stickney, *Electrochim. Acta*, **53**, 6157 (2008).
15. M. B. Vukmirovic, J. Zhang, K. Sasaki, A. U. Nilekar, F. Uribe, M. Mavrikakis, R. R. Adzic, *Electrochim. Acta*, **52**, 2257 (2007).
16. T. S. Mkwizu, M. K. Mathe, I. Cukrowski, *Manuscript submitted for publication*, (2009).
17. C.W. Bale, P. Chartrand, S.A. Degterov, G. Eriksson, K. Hack, R. Ben Mahfoud, J. Melançon, A.D. Pelton, and S. Petersen, *Calphad*, **26**, 189 (2002).
18. A. Bard, L. R. Faulkner, *Electrochemical methods: Fundamentals and Applications*, p. 603, John-Wiley & Sons, Inc, Danvers, USA (2001).
19. C. L. Green, A. Kucernak, *J. Phys. Chem. B* **106**, 11446 (2002).
20. E. Herrero, L. J. Buller, H. D. Abruna, *Chem. Rev.*, **101**, 1897 (2001).
21. C. L. Green, A. Kucernak, *J. Phys. Chem. B*, **106**, 1036 (2002).
22. T. Zapryanova, A. Hrussanova, A. Milchev, *J. Electroanal Chem.*, **600**, 311 (2007).
23. M. Van Brussel, G. Kokkinidis, I. Vandendael, C. Buess-Herman, *Electrochem. Comm.*, **4**, 808 (2002).
24. S. Trasatti, O. A. Petrii, *J. Electroanal. Chem.*, **327**, 353 (1992).
25. S. Hadzi-Jordanov, H. Angerstein-Kozlowska, M. Vukovic, B. E. Conway, *J. Electrochem. Soc.*, **125**, 1471 (1978).
26. J. G. Xu, X. W. Wang, *Surf. Sci.* **408**, 317 (1998).
27. O. A. Petrii, *J. Solid State Electrochem.*, **12**, 609 (2008).
28. J. Zhang, H. Ma, D. Zhang, P. liu, F. Tian, and Y. Ding, *Phys. Chem. Chem. Phys.*, **10**, 3250 (2008).
29. T. Frelink, W. Visscher, J. A. R. van Veen, *Surf. Sci.*, **335**, 353 (1995).
30. C.-G. Lee, M. Umeda, I. Uchida, *J. Power Sources*, **160**, 78 (2006).